High-Throughput and Comprehensive Prediction of H_2 Adsorption in Metal-Organic Frameworks Under Various Conditions

Yu Liu, Shuangliang Zhao, Honglai Liu, and Ying Hu
Dept. of Chemical Engineering, State Key Laboratory of Chemical Engineering, East China University of Science and Technology, Shanghai 200237, China

DOI 10.1002/aic.14842
Published online August 7, 2015 in Wiley Online Library (wileyonlinelibrary.com)

High-throughput prediction of H_2 adsorption in metal-organic framework (MOF) materials has been extended from a few specific conditions to the whole T, p space. The prediction is based on a classical density functional theory and has been implemented over 712 MOFs in 441 different conditions covering a wide range. Some testing materials show excellent behavior at low temperatures and obvious improvement at high temperatures compared to conventional MOFs. The structures of the best MOFs at high and low temperatures are totally different. Linear and nonlinear correlations between the two Langmuir parameters have been found at high and low temperatures, respectively. According to the analysis of the excess uptake, we found that the saturated pressure increases along with temperature in the low temperature region but decreases in the high temperature region. © 2015 American Institute of Chemical Engineers *AIChE J*, 61: 2951–2957, 2015

Keywords: adsorption, thermodynamics, statistical mechanics, metal-organic framework, classical density functional theory

Introduction

Metal-organic framework (MOF), as a high performance nanoporous material, has achieved great success in adsorption, separation, catalysis and sensing due to its high surface area, porosity and diversity.[1–18] In the adsorption field, specifically, gas storage is the most important application. During previous decades, thousands of structures have been proposed and synthesized, most of which are very satisfactory, such as MOF-177 [19] and NU-100.[20] However, as indicated by Snurr et al.,[21] there are millions or even billions of possible MOFs in principle, and it is reasonable to expect that there are many higher performance materials that exist in the unexploited region.

To address such a large number of materials, an efficient predictive method is expected. The traditional technique is the Monte Carlo simulation. One of the most impressive studies was performed by Snurr et al.,[21–26] who examined methane adsorption in 137,000 MOFs and identified over 300 structures that have a higher uptake than any known materials at a specified temperature and pressure. However, in real applications, due to the different demands of adsorption materials, adsorption properties at various conditions should be considered when evaluating a material. Hydrogen delivery is a typical example. One important issue, according to the US Department of Energy,[27] who stated that "infrastructure includes the pipelines, trucks, storage facilities, compressors, and dispensers involved in the process of delivering fuel," is that the delivery condition is related to a wide temperature and pressure range of 233–358 K and 0.3–1.2 MPa, respectively, in addition to the relevant storage condition.[28] In general, uptake under a specified condition may not reveal the expanse of a material. A more comprehensive prediction is required. To do this, we need to expand the predictions from several points (specified T, p) to the whole space (all reasonable T, p combinations). In this way, simulation may be not the best choice due to its high computational costs; thus, a more efficient method is expected.

The classical density functional theory (CDFT) may be the appropriate choice. The main idea of the CDFT is to obtain microscopic information (density profile) by minimizing the grand potential and to then obtain the thermodynamic properties from the density profile. During its 30 years of development, the accuracy and efficiency of the CDFT have been well-examined and improved, especially for adsorption systems.[29–40] Very recently, the CDFT has been successfully implemented for the fast screening of hydrogen storage in MOF materials at specified conditions and has produced similar results with a much lower computational cost compared to simulations.[41] In this work, we will extend the method into a full T, p space to give a comprehensive prediction of the adsorption properties.

Additional Supporting Information may be found in the online version of this article.

Correspondence concerning this article should be addressed to H. Liu at hlliu@ecust.edu.cn.

Molecular Model

We consider H_2 (guest) adsorbed in an MOF (host). Atom–atom interactions are modeled by a spherical Lennard-Jones (LJ) 12-6 potential

$$u_{ij}(\mathbf{r})=4\varepsilon_{ij}\left[\left(\frac{\sigma_{ij}}{r}\right)^{12}-\left(\frac{\sigma_{ij}}{r}\right)^{6}\right] \tag{1}$$

where ε_{ij} and σ_{ij} are the well depth and diameter between atoms i and j. The two parameters are obtained from the Lorentz–Berthelot mixing rule and the corresponding standard force fields. For H_2, $\varepsilon_{H2H2}/k_B = 36.7$ K, $\sigma_{H2H2} = 0.2958$ nm[42] (k_B is the Boltzmann constant); for MOF atoms, the universal force field[43] is used. The MOF structure is supposed to be rigid, that is, the host–host interactions can be regarded as a constant in the calculation. The coordinates of the MOF atoms are generated from the Northwestern hypothetic MOF database.[21]

Classical density functional theory

The CDFT starts from the grand potential, which can be written from its definition

$$\Omega[\rho(\mathbf{r})]=F[\rho(\mathbf{r})]-\mu\int\rho(\mathbf{r})\mathrm{d}\mathbf{r} \tag{2}$$

where $\rho(\mathbf{r})$ is the density profile of the guest molecule (H_2 in this work) and μ is the chemical potential, which can be obtained from the corresponding bulk system due to the equilibrium condition

$$\mu=\mu_{\mathrm{bulk}}(p,T) \tag{3}$$

where p, T are the pressure and temperature, respectively, and μ_{bulk} is the chemical potential of the bulk system, which can be calculated from the modified Benedict–Webb–Rubin (MBWR) equation of state.[44] $F[\rho(\mathbf{r})]$ is the free energy functional of density profile $\rho(\mathbf{r})$, which can be divided into ideal gas F^{id}, excessive F^{ex}, and external parts F^{ext}

$$F[\rho(\mathbf{r})]=F^{\mathrm{id}}[\rho(\mathbf{r})]+F^{\mathrm{ex}}[\rho(\mathbf{r})]+F^{\mathrm{ext}}[\rho(\mathbf{r})] \tag{4}$$

The ideal term stands for the kinetic contribution, which can be exactly written as

$$F^{\mathrm{id}}[\rho(\mathbf{r})]=k_BT\int\rho(\mathbf{r})[\ln\rho(\mathbf{r})-1]\mathrm{d}\mathbf{r} \tag{5}$$

The external term stands for the H_2-MOF interactions, which can also be expressed simply as

$$F^{\mathrm{ext}}[\rho(\mathbf{r})]=\int\rho(\mathbf{r})V^{\mathrm{ext}}(\mathbf{r})\mathrm{d}\mathbf{r} \tag{6}$$

$V^{\mathrm{ext}}(\mathbf{r})$ is the external potential, which can be calculated through the summation of host-guest (H_2-MOF interaction in this work) interactions

$$V^{\mathrm{ext}}(\mathbf{r})=\sum_{i\in\mathrm{MOF}}u_{i\mathrm{H}_2}(\mathbf{r}-\mathbf{r}_i) \tag{7}$$

where $\mathbf{r}_i$ represents the coordinates of the ith MOF atoms. The excess term arises from the guest–guest interactions, which cannot be expressed exactly. In this work, F^{ex} is approximated by a combination of three methods: the modified fundamental measure theory (MFMT), the weighted density approximation (WDA) and the mean field theory (MFT). The accuracy of this approximation has been well-examined in the previous work.[41] Specifically, the three methods are used to approximate the three terms contained in F^{ex}: the hard sphere term F^{hs}, the correlation term F^{cor}, and the attractive term F^{attr}, respectively

$$F^{\mathrm{ex}}[\rho(\mathbf{r})]=F^{\mathrm{hs}}[\rho(\mathbf{r})]+F^{\mathrm{cor}}[\rho(\mathbf{r})]+F^{\mathrm{attr}}[\rho(\mathbf{r})] \tag{8}$$

Equation 8 is straight forward for hard sphere-attractive models; the LJ 12-6 model can be modified into a hard sphere-attraction model by the Barker Henderson theory[45]

$$u^{\mathrm{LJ}}(r)=u^{\mathrm{hs}}(r)+u^{\mathrm{attr}}(r) \tag{9}$$

where

$$u^{\mathrm{hs}}(r)=\begin{cases}\infty & r<d\\ 0 & r>d\end{cases} \tag{10}$$

and

$$u^{\mathrm{attr}}(r)=\begin{cases}0 & r<\sigma\\ 4\varepsilon\left[\left(\frac{\sigma}{r}\right)^{12}-\left(\frac{\sigma}{r}\right)^{6}\right] & r>\sigma\end{cases} \tag{11}$$

where d is the hard sphere diameter, which can be calculated using

$$d=\frac{1+0.2977(\beta\varepsilon)^{-1}}{1+0.33163(\beta\varepsilon)^{-1}+0.0010477(\beta\varepsilon)^{-2}}\sigma \tag{12}$$

with $\beta = 1/(k_BT)$.

With such a modification, Eq. 8 can be calculated item by item: first, the hard sphere term is calculated using the MFMT[33]

$$\beta F^{\mathrm{hs}}=\int\Phi^{\mathrm{hs}}[n_\alpha(\mathbf{r})]\mathrm{d}\mathbf{r} \tag{13}$$

$$\begin{aligned}\Phi^{\mathrm{hs}}=&-n_0\ln(1-n_3)+\frac{n_1n_2-\boldsymbol{n}_{\mathrm{V1}}\cdot\boldsymbol{n}_{\mathrm{V2}}}{1-n_3}\\&+\frac{n_3+(1-n_3)^2\ln(1-n_3)}{36\pi n_3^2(1-n_3)^2}(n_2^3-3n_2\boldsymbol{n}_{\mathrm{V2}}\cdot\boldsymbol{n}_{\mathrm{V2}})\end{aligned} \tag{14}$$

$$n_\alpha(\mathbf{r})=\int\rho(\mathbf{r}')w^{(\alpha)}(|\mathbf{r}-\mathbf{r}'|)\mathrm{d}\mathbf{r}'\quad\alpha\in\{0,1,2,3,\mathrm{V1},\mathrm{V2}\} \tag{15}$$

$w^{(\alpha)}$ are the weighting functions, which can be expressed as

$$\begin{cases}w^{(2)}(r)=\pi d^2w^{(0)}(r)=2\pi dw^{(1)}(r)=\delta(d/2-r)\\ w^{(3)}(r)=\theta(d/2-r)\\ \boldsymbol{w}^{(\mathrm{V2})}(\mathbf{r})=2\pi d\boldsymbol{w}^{(\mathrm{V1})}(\mathbf{r})=w^{(2)}(r)\dfrac{\mathbf{r}}{r}\end{cases} \tag{16}$$

where $\delta(r)$ is the Dirac function and $\theta(r)$ is the Heaviside step function.

Second, the attractive term, F^{attr}, is written using MFT

$$F^{\mathrm{attr}}=\frac{1}{2}\int\int\rho(\mathbf{r})\rho(\mathbf{r}')u^{\mathrm{attr}}(\mathbf{r}-\mathbf{r}')\mathrm{d}\mathbf{r}\mathrm{d}\mathbf{r}' \tag{17}$$

Third, the correlation term, F^{cor}, is calculated using WDA

$$F^{\mathrm{cor}}=\int\rho(\boldsymbol{r})f^{\mathrm{cor}}[\bar{\rho}(\mathbf{r})]\mathrm{d}\mathbf{r} \tag{18}$$

where $\bar{\rho}(\mathbf{r})$ is the weighted density

$$\bar{\rho}(\mathbf{r})=\frac{3}{4\pi d^3}\int\rho(\mathbf{r}')\theta(d-|\mathbf{r}-\mathbf{r}'|)\mathrm{d}\mathbf{r}' \tag{19}$$

and $f^{cor}(\rho)$ is the bulk free energy density (per number of molecules) due to the correlation effect, which can be obtained by

$$f^{cor}(\rho)=\frac{F^{LJ}_{bulk}(\rho)}{N}-\frac{F^{hs}_{bulk}(\rho)}{N}-\frac{F^{MFA}_{bulk}(\rho)}{N} \tag{20}$$

where N is the number of molecules and $F^{LJ}_{bulk}(\rho)$ is the excess free energy for bulk LJ fluid, which is obtained using the MBWR equation of state[44]

$$\frac{F^{LJ}_{bulk}(\rho)}{N}=\varepsilon\left(\sum_{i=1}^{8}\frac{a_i\rho^i\sigma^{3i}}{i}+\sum_{i=1}^{6}b_iG_i\right) \tag{21}$$

where a_i and b_i are functions of T and G_i are functions of $\rho\sigma^3$. $F^{hs}_{bulk}(\rho)$ is the excess free energy for bulk hard sphere fluid, which can be obtained from the Carnahan–Starling (CS) equation of state[46]

$$\frac{F^{hs}_{bulk}(\rho)}{N}=k_BT\frac{4\eta-3\eta^2}{(1-\eta)^2} \tag{22}$$

$F^{MFA}_{bulk}(\rho)$ is the attractive term defined by Eq. 17 when $\rho(\mathbf{r})$ trends to ρ, which takes the form

$$\frac{F^{MFA}_{bulk}(\rho)}{N}=-\frac{16}{9}\pi\beta\varepsilon\rho\sigma^3 \tag{23}$$

According to Eqs. 2–23, grand potential Ω can be written as a functional of density profile, $\Omega[\rho(\boldsymbol{r})]$. By minimizing $\Omega[\rho(\mathbf{r})]$, the three-dimensional (3-D) density profile $\rho(\mathbf{r})$ can be obtained. For an adsorption system, the uptake N_{ads} can then be calculated from the integration of $\rho(\mathbf{r})$

$$N_{ads}=\int\rho(\mathbf{r})d\mathbf{r} \tag{24}$$

Computational Methods

All calculations are given in a 3-D box with a periodical boundary condition and a grid resolution of 0.05 nm. The cutoff distance of the LJ potential is set at 1.3 nm, and the box length is two times larger than the cutoff distance, depending on the unit cell of MOFs. Fast Fourier transform (FFTW3 package[47]) is used to compute all convolutions in the CDFT: (such as Eqs. 15, 17, and 19)

$$\int f_1(\mathbf{r})f_2(\mathbf{r}-\mathbf{r}')d\mathbf{r}'=\mathcal{F}^{-1}\{\mathcal{F}[f_1(\mathbf{r})]\mathcal{F}[f_2(\mathbf{r})]\} \tag{25}$$

where $\mathcal{F}$ and $\mathcal{F}^{-1}$ stand for the forward and backward fast Fourier transform, respectively. A conjugate gradient method (CG_DESENT package[48,49]) is used for minimizing the grand potential.

We picked up 712 types of MOF materials that give the highest uptake in a previously specified screening (the detailed structure codes are listed in the supporting information).[21,41] For each material, the prediction is implemented under 441 different conditions (21×21 in T, p space) with a temperature range from 77 to 373 K and a pressure range from 1 kPa to 10 MPa. The whole calculation ($712 \times 441 = 313{,}992$ cases in total) only takes approximately 1500 CPU hours.

Results and Discussion

Uptake is always the essential concern for adsorption; Figure 1 shows the highest uptake (N_{max}) among the 712 structures under 441 different conditions. Clearly, the most impressive uptakes are located in the lower temperature region. Specifically, at 77 K, the highest uptake at 10 MPa reaches 38 mol/L, which is higher than MOF-177 [50] by 10% and exceeds the density of liquid hydrogen (35 mol/L). Even at very low pressure, for example, 1 kPa, the uptake also reaches 13 mol/L, a value comparable to the saturated uptake of many known MOFs.[50] In contrast, at high temperatures, for example, 298 K, although the values are not as impressive as those at low temperatures, improvement can also be found compared to current MOFs.[51] Obviously, decreasing the uptake along the T axis is much faster than that along the p axis; the uptake at 77 K and 1 kPa is two times the uptake at 298 K and 10 MPa. This indicates that storing H_2 at low temperatures is more efficient and preferable than at high pressures.

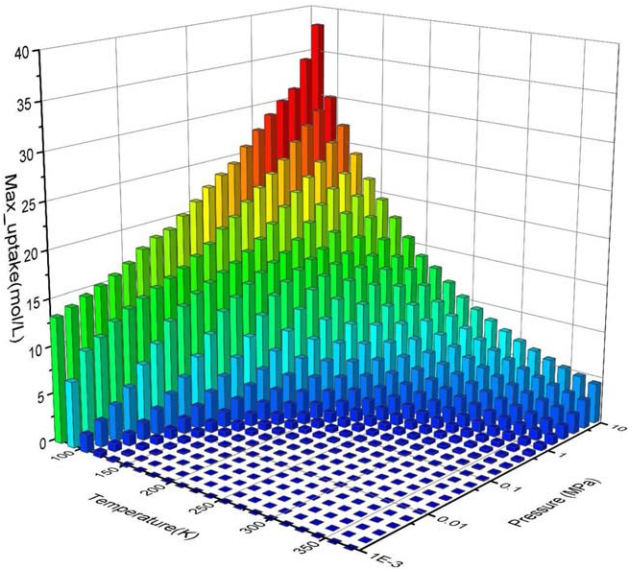

Figure 1. The highest uptakes from 712 types of MOF materials at different temperature and pressure.

[Color figure can be viewed in the online issue, which is available at wileyonlinelibrary.com.]

To identify the most successful structures, in Table 1, we list the top 10 materials that give the highest uptake under four typical conditions: 298 K and 0.1 MPa, 298 K and 10 MPa, 77 K and 0.1 MPa, and 77 K and 10 MPa. It seems that the finalists for 298 K and 0.1 MPa and 298 K and 10 MPa are very similar, and the structure with code 254 gives the highest uptake for both cases. The reason may lie in the similar slopes of the nearly linear isotherms, which will be shown later. For the condition of 77 K, the situation is completely different. At 0.1 MPa, four new structures (with codes 215, 216, 311, 360) have arisen, and the structure with code 216 emerges as the best one. However, at 10 MPa, the finalists are totally different; none of the candidates can be found in the foregoing lists. Such differences indicate that screening in a fixed condition is inadequate to evaluate a material. To give insight, we picked up three structures that show the highest uptake in the four conditions: structures 254, 216, and 401. The isotherms and their Langmuir fitting can be found in Figures 2a, b, while the corresponding structures are shown in Figure 2c. Figure 2a shows the isotherms at a high temperature of 298K, which display a trend of near

Table 1. Top 10 MOF Structures for H_2 Adsorption Under Different Conditions (Uptake Unit: mol/L)

	298K, 0.1 MPa		298 K, 10 MPa		77K, 0.1 MPa		77K, 10 MPa	
Order	Code	Uptake	Code	Uptake	Code	Uptake	Code	Uptake
1	254	0.1451	254	6.818	216	21.33	401	37.94
2	226	0.1432	226	6.727	227	21.27	399	37.89
3	231	0.1419	231	6.613	252	19.98	373	36.64
4	258	0.1273	207	6.515	215	19.80	409	36.27
5	298	0.1270	258	6.413	254	19.79	21	33.12
6	342	0.1241	298	6.391	207	19.74	17	33.08
7	207	0.1225	232	6.333	311	19.46	18	33.08
8	232	0.1210	222	6.263	222	19.37	11	33.07
9	222	0.1181	292	6.140	258	19.30	20	33.04
10	292	0.1140	227	6.136	360	19.18	1	33.03

linearity with similar slopes for different materials; Figure 2b depicts the isotherms at a low temperature of 77 K with remarkably different shapes for different MOFs. By comparing these three figures, it is easy to find the correlations between the isotherms and the structures; structures with high surface area give higher uptake in a medium or relatively low loading region, while structures with a large pore size result in a higher uptake in a high loading region. This is consistent with Frost et al.'s finding:[52] the uptake is correlated with the heat of adsorption, surface area and free volume at low, intermediate and high loadings, respectively. In most cases, there are three typical adsorption areas in an MOF material (sorted by the binding strength): the favorable adsorption sites (usually around the metal sites), surface and pore center. For the low uptake case, guest molecules are mainly adsorbed at the favorable sites and the uptake depends on the binding strength between metal sites and guest molecules, which is represented by the heat of adsorption in the macroscopic view; once the favorable sites are saturated, guest molecules tend to stay at the surface, and the surface area dominates the uptake; finally, if both are saturated, the uptake is determined by how much free volume is available. Such a microscopic mechanism has also been exhibited in other studies.[53,54]

Clearly, the isotherms in Figures 2a, b could be fitted very well by the Langmuir equation

$$N_{\text{ads}} = N_0 \frac{p}{p+p_0} \tag{26}$$

where N_{ads} stands for uptake, p for pressure, and p_0, N_0 are two fitting parameters. The two parameters capture the essential properties of the adsorption isotherm, where N_0 is

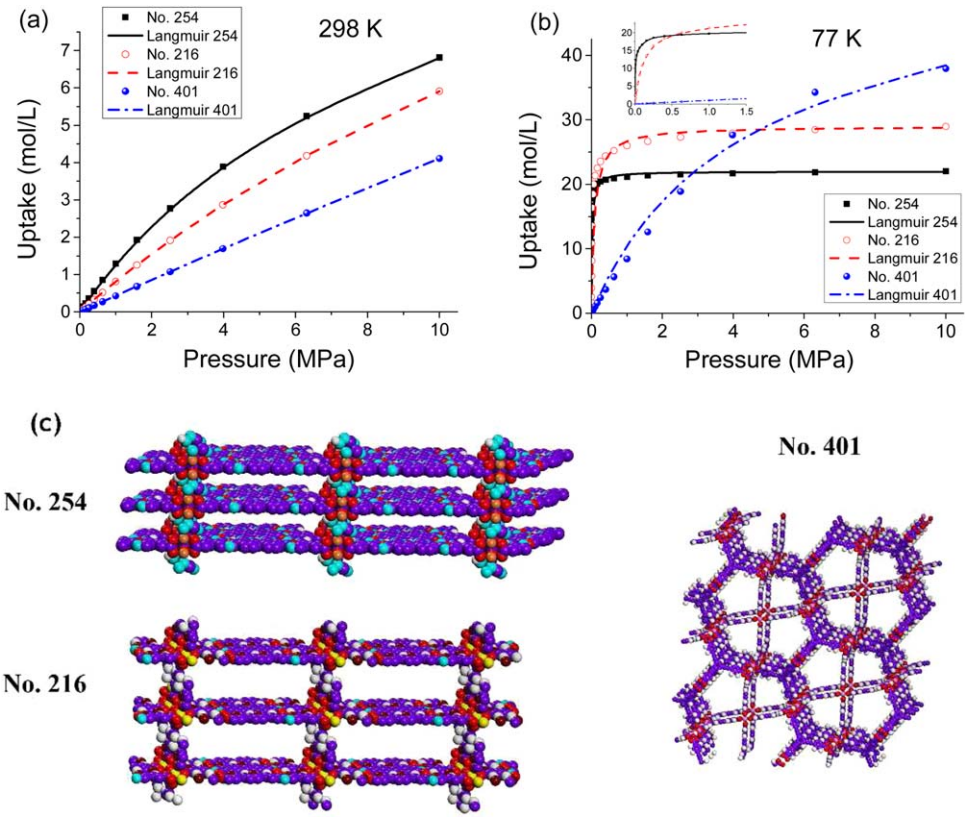

Figure 2. Adsorption isotherms for three MOF structures (with codes 254, 216, 401, respectively) at (a) 298 K; (b) 77 K.

(c) Structure of the three MOFs, with color codes: C, purple; H, white; O, red; N, light blue; Zn, pink; Cu, orange; Br, wine; V, yellow. [Color figure can be viewed in the online issue, which is available at wileyonlinelibrary.com.]

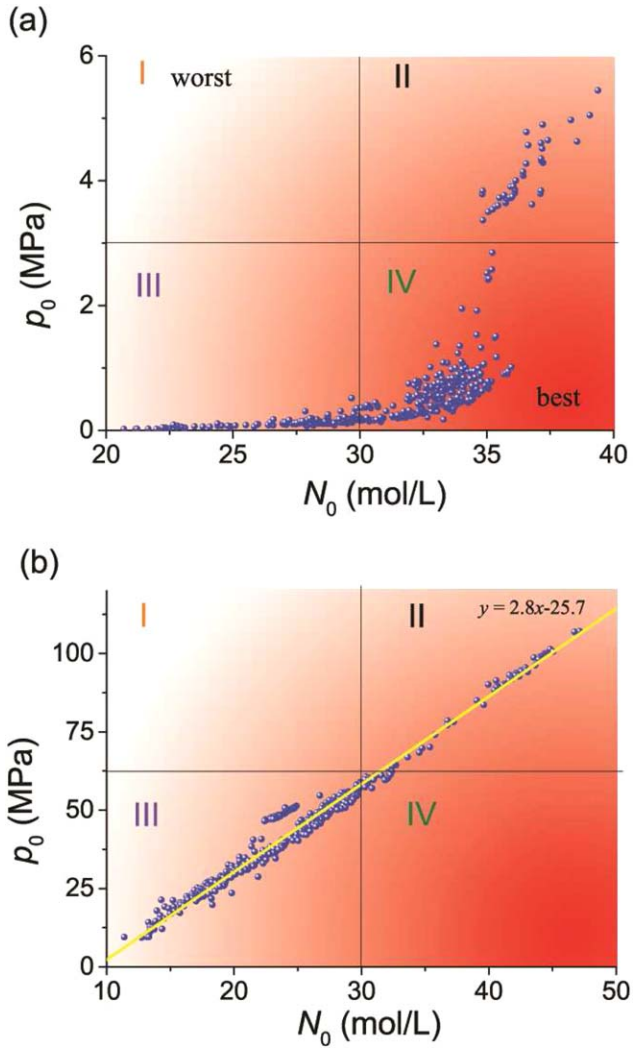

Figure 3. Langmuir parameters of 712 types of MOF material at (a) low (77 K) and (b) high (298 K) temperatures.

The line in (b) is a numerical fitting result. [Color figure can be viewed in the online issue, which is available at wileyonlinelibrary.com.]

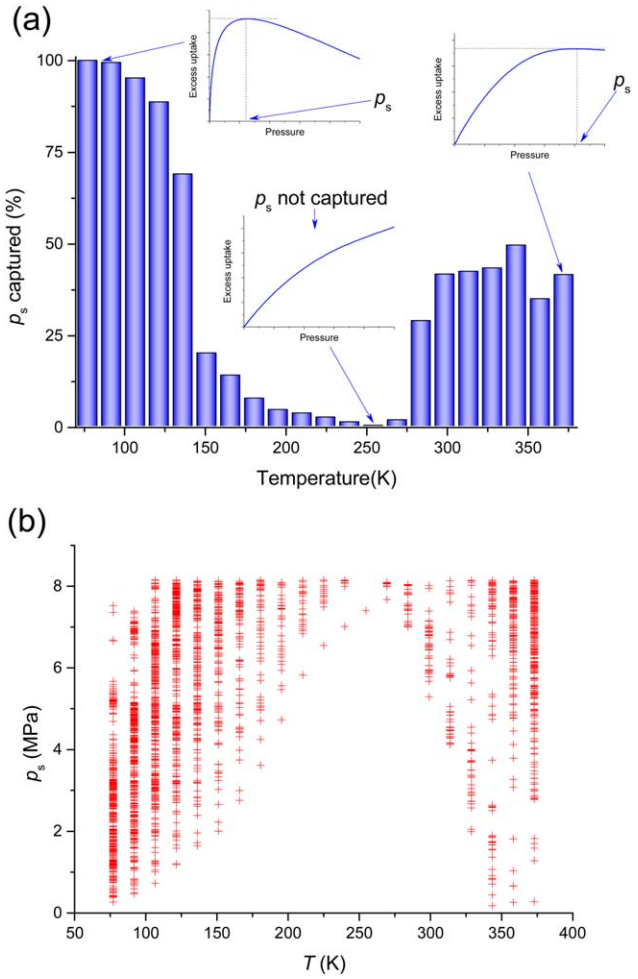

Figure 4. Saturated pressure p_s at different temperatures: (a) percentage of how many p_s are captured in the range of 1 kPa–10 MPa; the three subfigures are the excess uptake isotherms of a typical structure (code 6) at temperatures 77 K, 250 K, and 373 K, respectively.

(b) Saturated pressure p_s at different temperatures. [Color figure can be viewed in the online issue, which is available at wileyonlinelibrary.com.]

the saturated uptake, which is determined by the free volume, and p_0 denotes the linear region of the isotherm, which is inversely proportional to the binding strength. We fit p_0 and N_0 for all 712 MOFs at different temperatures. Figure 3 shows the results at two typical temperatures: 77 and 298 K. The N_0-p_0 space can be separated into four regions, as marked. For gas storage, high N_0 and low p_0 are favorable, which means that materials located at the bottom right corner, denoted as region IV, should be the best ones. Second, materials in region II give high N_0 and high p_0, which implies that the materials may be favorable at high pressure. Correspondingly, materials in region III may be promising at low pressure. Region I denotes the worst materials for gas storage. For the low temperature case, as shown in Figure 3a, most materials are located in region IV and none are located in region I, which suggests that all these testing materials are promising for low temperature and most of them should be very successful. At high temperature, as shown in Figure 3b, the behavior is different. A linear relation between p_0 and N_0 seems to be exhibited. According to their physical meaning, this suggests that the larger the free volume is, the weaker the binding strength. Because the attraction between H_2 and an MOF atom is relatively weak (compared to kinetic energy) at high temperatures, the binding strength is determined by the density of MOF atoms. To strengthen the binding energy, one has to make the pore size smaller (such as structure 254, shown in Figure 2c), which leads to a smaller free volume, and finally, a correlation is formed between p_0 and N_0. For low temperature, the binding strength is better determined by the well depth of the site–site attractions, which breaks down the linearity.

Figure 4 shows the saturated pressure for different materials and temperatures. The excess uptake is defined by the uptake differences between the adsorbed phase and bulk phase, that is, $N_{ex} = N_{ads} - N_b$, where N_b is the number of guest molecules (H_2) in the bulk phase. Because N_b is independent of the MOF structures, screening based on absolute uptake N_{ads} and N_{ex} is equivalent; however, to examine the

saturated adsorption, the peak of excess uptake is more convincing than the numerically fitted parameters in many cases. In this work, the saturated pressure p_s is defined as the corresponding pressure at the peak of the excess uptake isotherm. Due to the restriction of our calculation range, we can capture p_s only when 1 kPa $< p_s <$ 10 MPa. Figure 4a shows how many p_s are found from 1 kPa–10 MPa (by percentage). Figure 4b shows the values of the saturated pressure p_s at different temperatures. According to the definition, p_s denotes the attractive-repulsive transition point of the adsorbent, that is, when $p < p_s$, the adsorbent is attractive, and when $p > p_s$, the adsorbent becomes repulsive. Because N_b is larger than N_{ads} (i.e., $N_{ex} < 0$) when $p \to \infty$, in principle, there should be a peak for each isotherm. For the uncaptured one, the peak could locate at $p_s >$ 10 MPa. For the low temperature case of 77 K, all materials are saturated during adsorption when $p_s <$ 8 MPa and most of the saturated pressures are located at $p_s <$ 4 MPa, as shown in Figure 4b. For the high temperature cases, that is, $T >$ 300 K, approximately 30% of the peaks are captured and most of them are located in the high pressure region. Something special happens in the medium temperature region, that is, 150 K $< T <$ 270 K, where most peaks are not captured, that is, $p_s >$ 10 MPa. This suggests an increase-decrease trend of $p_s(T)$. The increase of $p_s(T)$ can be understood by the filling of free volume; when temperature increases, higher pressure is required to fill up the free volume. The decrease is due to the weak host-guest attraction at high temperature. In this case, only the favorable sites are attractive; once these sites are occupied, the entire MOF becomes repulsive and the gases tend to stay in the bulk, and the increase of N_{ads} cannot keep up with the increase of N_b, even though there is much free volume available, that is, $\left(\frac{dN_{ex}}{dp}\right)_T = \left(\frac{dN_{ads}}{dp}\right)_T - \left(\frac{dN_b}{dp}\right)_T < 0$ is satisfied in the low pressure region. In other words, at p_s, the material is not really "saturated" because there is still much free volume left; what p_s really stands for is the attractive-repulsive transition. The higher the temperature is, the weaker the attraction and the less gas molecules required to make MOF repulsive; this leads to the decreasing trend of $p_s(T)$ in the high temperature region.

Conclusion

A fast and comprehensive prediction of H_2 adsorption over 712 MOF materials and 441 different conditions has been implemented using the CDFT. According to the predictions, the following elements have been found: first, the materials show excellent performance at low temperatures and obvious improvement at high temperatures compared to current MOFs. Second, the characteristics of the best structures at high and low temperatures are completely different. Third, correlations between the two Langmuir parameters and an increase-decrease trend in $p_s(T)$ have been captured and explained.

Acknowledgments

This work is supported by the National Basic Research Program of China (2013CB733501), the National Natural Science Foundation of China (No. 91334203 and 21206036), the 111 Project of Ministry of Education of China (No. B08021), the Open Project of State Key Laboratory of Chemical Engineering of China (SKL-ChE-13C04), and the Fundamental Research Funds for the Central Universities.

Literature Cited

1. Rosseinsky MJ. Recent developments in metal-organic framework chemistry: design, discovery, permanent porosity and flexibility. *Microporous Mesoporous Mater*. 2004;73(1–2):15–30.
2. Bauer CA, Timofeeva TV, Settersten TB, Patterson BD, Liu VH, Simmons BA, Allendorf MD. Influence of connectivity and porosity on ligand-based luminescence in zinc metal-organic frameworks. *J Am Chem Soc*. 2007;129(22):7136–7144.
3. Ma L, Jin A, Xie Z, Lin W. Freeze drying significantly increases permanent porosity and hydrogen uptake in 4,4-connected metal-organic frameworks. *Angew Chem Int Ed*. 2009;48(52):9905–9908.
4. Furukawa H, Ko N, Go YB, Aratani N, Choi SB, Choi E, Yazaydin AO, Snurr RQ, O'Keeffe M, Kim J, Yaghi OM. Ultrahigh porosity in metal-organic frameworks. *Science*. 2010;329(5990):424–428.
5. Yazaydin AO, Snurr RQ, Park TH, et al. Screening of metal-organic frameworks for carbon dioxide capture from flue gas using a combined experimental and modeling approach. *J Am Chem Soc*. 2009; 131(51):18198–18199.
6. Cychosz KA, Wong-Foy AG, Matzger AJ. Liquid phase adsorption by microporous coordination polymers: removal of organosulfur compounds. *J Am Chem Soc*. 2008;130(22):6938–6939.
7. Farha OK, Yazaydin AO, Eryazici I, Malliakas CD, Hauser BG, Kanatzidis MG, Nguyen ST, Snurr RQ, Hupp JT. De novo synthesis of a metal-organic framework material featuring ultrahigh surface area and gas storage capacities. *Nat Chem*. 2010;2(11):944–948.
8. Li H, Eddaoudi M, O'Keeffe M, Yaghi OM. Design and synthesis of an exceptionally stable and highly porous metal-organic framework. *Nature*. 1999;402(6759):276–279.
9. Eddaoudi M, Moler DB, Li HL, Chen BL, Reineke TM, O'Keeffe M, Yaghi OM. Modular chemistry: secondary building units as a basis for the design of highly porous and robust metal-organic carboxylate frameworks. *Acc Chem Res*. 2001;34(4):319–330.
10. Rosi NL, Eckert J, Eddaoudi M, Vodak DT, Kim J, O'Keeffe M, Yaghi OM. Hydrogen storage in microporous metal-organic frameworks. *Science*. 2003;300(5622):1127–1129.
11. Ma L, Abney C, Lin W. Enantioselective catalysis with homochiral metal-organic frameworks. *Chem Soc Rev*. 2009;38(5):1248–1256.
12. Corma A, Garcia H, Llabres i Xamena FXLI. Engineering metal organic frameworks for heterogeneous catalysis. *Chem Rev*. 2010; 110(8):4606–4655.
13. Li J-R, Sculley J, Zhou H-C. Metal-organic frameworks for separations. *Chem Rev*. 2012;112(2):869–932.
14. Kreno LE, Leong K, Farha OK, Allendorf M, Van Duyne RP, Hupp JT. Metal-organic framework materials as chemical sensors. *Chem Rev*. 2012;112(2):1105–1125.
15. Suh MP, Park HJ, Prasad TK, Lim D-W. Hydrogen storage in metal-organic frameworks. *Chem Rev*. 2012;112(2):782–835.
16. Peng Y, Gong T, Zhang K, Lin X, Liu Y, Jiang J, Cui Y. Engineering chiral porous metal-organic frameworks for enantioselective adsorption and separation. *Nat Commun*. 2014;5:4406.
17. Zhang L, Hu Z, Jiang J. Sorption-induced structural transition of zeolitic imidazolate framework-8: a hybrid molecular simulation study. *J Am Chem Soc*. 2013;135(9):3722–3728.
18. Peng X, Cao D. Computational screening of porous carbons, zeolites, and metal organic frameworks for desulfurization and decarburization of biogas, natural gas, and flue gas. *AIChE J*. 2013;59(8): 2928–2942.
19. Chae HK, Siberio-Perez DY, Kim J, Go Y, Eddaoudi M, Matzger AJ, O'Keeffe M, Yaghi OM. A route to high surface area, porosity and inclusion of large molecules in crystals. *Nature*. 2004; 427(6974):523–527.
20. Farha OK, Özgür Yazaydın A, Eryazici I, et al. De novo synthesis of a metal–organic framework material featuring ultrahigh surface area and gas storage capacities. *Nat Chem*. 2010;2(11):944–948.
21. Wilmer CE, Leaf M, Lee CY, Farha OK, Hauser BG, Hupp JT, Snurr RQ. Large-scale screening of hypothetical metal-organic frameworks. *Nat Chem*. 2012;4(2):83–89.
22. Walton KS, Millward AR, Dubbeldam D, Frost H, Low JJ, Yaghi OM, Snurr RQ. Understanding inflections and steps in carbon dioxide adsorption isotherms in metal-organic frameworks. *J Am Chem Soc*. 2008;130(2):406–407.
23. Colon YJ, Snurr RQ. High-throughput computational screening of metal-organic frameworks. *Chem Soc Rev*. 2014;43(16):5735–5749.
24. Gomez-Gualdron DA, Wilmer CE, Farha OK, Hupp JT, Snurr RQ. Exploring the limits of methane storage and delivery in nanoporous materials. *J Phys Chem C*. 2014;118(13):6941–6951.

25. Snurr RQ, Hupp JT, Nguyen ST. Prospects for nanoporous metal-organic materials in advanced separations processes. *AIChE J*. 2004; 50(6):1090–1095.
26. Ryan P, Farha OK, Broadbelt LJ, Snurr RQ. Computational screening of metal-organic frameworks for xenon/krypton separation. *AIChE J*. 2011;57(7):1759–1766.
27. Available at: http://energy.gov/eere/fuelcells/hydrogen-delivery. 2014.
28. Langmi HW, Ren J, North B, Mathe M, Bessarabov D. Hydrogen storage in metal-organic frameworks: a review. *Electrochim Acta*. 2014;128:368–392.
29. Rosenfeld Y. Free-energy model for the inhomogeneous hard-sphere fluid mixture and density-functional theory of freezing. *Phys Rev Lett*. 1989;63(9):980–983.
30. Kierlik E, Rosinberg ML. Density-functional theory for inhomogeneous fluids—adsorption of binary-mixtures. *Phys Rev A*. 1991;44(8): 5025–5037.
31. Rosenfeld Y. Free-energy model for inhomogeneous fluid mixtures: Yukawa-charged hard-spheres, general interactions, and plasmas. *J Chem Phys*. 1993;98(10):8126–8148.
32. Rosenfeld Y. Phase separation of asymmetric binary hard-sphere fluids: self-consistent density functional theory. *Phys Rev Lett*. 1994; 72(24):3831–3834.
33. Yu YX, Wu JZ. Structures of hard-sphere fluids from a modified fundamental-measure theory. *J Chem Phys*. 2002;117(22):10156–10164.
34. Li Z, Wu J. Density-functional theory for the structures and thermodynamic properties of highly asymmetric electrolyte and neutral component mixtures. *Phys Rev E*. 2004;70(3 Pt 1):031109.
35. Yu Y-X. A novel weighted density functional theory for adsorption, fluid-solid interfacial tension, and disjoining properties of simple liquid films on planar solid surfaces. *J Chem Phys*. 2009;131(2): 024704.
36. Liu Y, Liu HL, Hu Y, Jiang JW. Density functional theory for adsorption of gas mixtures in metal-organic frameworks. *J Phys Chem B*. 2010;114(8):2820–2827.
37. Liu Y, Zhao S, Wu J. A site density functional theory for water: application to solvation of amino acid side chains. *J Chem Theory Comput*. 2013;9(4):1896–1908.
38. Neimark AV, Ravikovitch PI. Capillary condensation in MMS and pore structure characterization. *Microporous Mesoporous Mater*. 2001;44:697–707.
39. Neimark AV, Ravikovitch PI, Vishnyakov A. Adsorption hysteresis in nanopores. *Phys Rev E*. 2000;62(2):R1493–R1496.
40. Vishnyakov A, Ravikovitch PI, Neimark AV. Molecular level models for CO2 sorption in nanopores. *Langmuir*. 1999;15(25):8736–8742.
41. Fu J, Liu Y, Tian Y, Wu J. Density functional methods for fast screening of metal-organic frameworks for hydrogen storage. *J Phys Chem C*. 2015;119(10):5374–5385.
42. Buch V, Devlin JP. Preferential adsorption of ortho-H 2 with respect to para-H 2 on the amorphous ice surface. *J Chem Phys*. 1993;98(5): 4195–4206.
43. Rappe AK, Casewit CJ, Colwell KS, Goddard WA, Skiff WM. UFF, a full periodic table force field for molecular mechanics and molecular dynamics simulations. *J Am Chem Soc*. 1992;114(25):10024–10035.
44. Johnson JK, John AZ, Keith EGD-LD. The Lennard-Jones equation of state revisited. *Mol Phys*. 1992;78(3):591–618.
45. Barker JA, Henderso D. Perturbation theory and equation of state for fluids. 2. a successful theory of liquids. *J Chem Phys*. 1967;47(11): 4714–4721.
46. Carnahan NF, Starling KE. Equation of state for nonattracting rigid spheres. *J Chem Phys*. 1969;51:635–636.
47. Frigo M, Johnson SG. The design and implementation of FFTW3. *Proc IEEE*. 2005;93(2):216–231.
48. Hager WW, Zhang HC. A new conjugate gradient method with guaranteed descent and an efficient line search. *SIAM J Optim*. 2005;16(1):170–192.
49. Hager WW, Zhang HC. Algorithm 851: CG DESCENT, a conjugate gradient method with guaranteed descent. *ACM Trans Math Softw*. 2006;32(1):113–137.
50. Wong-Foy AG, Matzger AJ, Yaghi OM. Exceptional H-2 saturation uptake in microporous metal-organic frameworks. *J Am Chem Soc*. 2006;128(11):3494–3495.
51. Kaye SS, Dailly A, Yaghi OM, Long JR. Impact of preparation and handling on the hydrogen storage properties of Zn4O(1,4-benzenedicarboxylate)3 (MOF-5). *J Am Chem Soc*. 2007;129(46):14176–14177.
52. Frost H, Düren T, Snurr RQ. Effects of surface area, free volume, and heat of adsorption on hydrogen uptake in metal−organic frameworks. *J Phys Chem B*. 2006;110(19):9565–9570.
53. Siderius DW, Gelb LD. Predicting gas adsorption in complex microporous and mesoporous materials using a new density functional theory of finely discretized lattice fluids. *Langmuir*. 2009;25(3): 1296–1299.
54. Liu Y, Liu HL, Hu Y, Jiang JW. Development of a density functional theory in three-dimensional nanoconfined space: H2 storage in metal organic frameworks. *J Phys Chem B*. 2009;113(36):12326–12331.

Manuscript received Dec. 31, 2014, and revision received Apr. 9, 2015.